# FATIGUE LIFE ANALYSIS OF TAPERED HYBRID COMPOSITE FLEXBEAMS

Gretchen B. Murri
*U.S. Army Research Laboratory, Vehicle Technology Directorate*
*NASA Langley Research C enter, Hampton, VA*

Jeffery R. Schaff
*United Technologies Research Center, East Hartford, CT*

Alan L. Dobyns
*Sikorsky Aircraft, Stratford, CT*

## ABSTRACT

Nonlinear-tapered flexbeam laminates from a full-size composite helicopter rotor hub flexbeam were tested under combined constant axial tension and cyclic bending loads. The two different graphite/glass hybrid configurations tested under cyclic loading failed by delamination in the tapered region. A 2-D finite element model was developed which closely approximated the flexbeam geometry, boundary conditions, and loading. The analysis results from two geometrically nonlinear finite element codes, ANSYS and ABAQUS, are presented and compared. Strain energy release rates (G) obtained from the above codes using the virtual crack closure technique (VCCT) at a resin crack location in the flexbeams are presented for both hybrid material types. These results compare well with each other and suggest that the initial delamination growth from the resin crack toward the thick region of the flexbeam is strongly mode II. The peak calculated G values were used with material characterization data to calculate fatigue life curves and compared with test data. A curve relating maximum surface strain to number of loading cycles at delamination onset compared reasonably well with the test results.

Key words: flexbeam, delamination, VCCT, fatigue, strain energy release rate, fracture mechanics

## INTRODUCTION

Polymeric composites are used to manufacture hingeless, bearingless composite rotor hubs for helicopters. These components are made of fewer parts and offer the advantages of reduced weight and drag, compared to metal hubs. However, unlike metals, there are no fracture mechanics based methods for predicting strength and life of these structures with damage. Typically, damage is simulated in structural analytical models and fracture mechanics based techniques are used to calculate strain energy release rates, as proposed by O'Brien in ref. 1 and summarized by Martin in ref. 2. In ref. 3, the fatigue life to onset of delamination was correctly calculated for coupon-size tapered flexbeams under tension-bending cyclic loading. An analysis and test methodology that incorporates damage, failure initiation and growth, and failure probability is critical to demonstrate reliability for new and existing rotor hub designs.

In order to accommodate bending loads in the flapping flexure region, composite flexbeams use internal ply-drops to create a non-linear taper. These internal ply-drops create material and geometric discontinuities, and are sources of delamination onset [3-8]. In ref. 9, the effect of combined tension-bending loading on two different hybrid graphite/glass-epoxy laminates with a nonlinear taper was studied. Test specimens were cut from a full-size helicopter tail-rotor flexbeam and were tested in a hydraulic load frame under combined constant axial-tension load and transverse cyclic bending loads. A 2-D finite element (FE) model of one of the hybrid layups was developed and combined axial tension and cyclic bending loading was applied. Delamination was simulated in the model to duplicate the observed delaminations from the experiments. The model was analyzed using both the ANSYS [10] and ABAQUS

[11] finite element codes. Strain energy release rate results from the two codes were compared for one hybrid type. The G-values from the two codes differed by approximately 8%.

In this study, strain energy release rates from both FE codes were calculated for both hybrid configurations using the virtual crack closure technique (VCCT) [12]. The strain energy release rate results were used to calculate delamination onset life. Additional coupon specimens were tested and fatigue lives were compared to the calculated results. The delamination growth in one specimen was monitored and recorded with the use of a computer-controlled high-speed camera.

## EXPERIMENTS

Specimen Geometry and Test Conditions

The flexibility requirements of the flexbeam are accomplished by varying the beam thickness and ply stacking sequences along its length. In the specimen shown in fig. 1, the thin center section has unidirectional plies, the tapered section is made of unidirectional and off-axis plies added in steps along the length, and the uniform thick section has unidirectional and off-axis plies.

Coupon-size specimens (shown in fig. 1) were cut from the outboard taper region of full size flexbeams from a commercial Sikorsky tail rotor. The specimens had a nonlinear taper design and were symmetric about the midplane. The specimen thickness varied from 129 plies at the thick end, to 39 plies at the thin end. The layup consisted of 0, 45, and -45 degree plies, with continuous 0-degree plies along the beam length. The ply terminations occurred in stepped pairs of either 45/-45 plies, or 4-ply groups of $[0_2/45/-45]$. The specimens were fabricated using a combination of S2/8552 glass/epoxy and IM7/8552 graphite/epoxy material systems. Material properties and nominal ply thickness for both materials are given in Table 1.

Table 1. Typical laminae room temperature properties.

| Material | $E_{1t}$, GPa (msi) | $E_{2t}$, GPa (msi) | $E_{1c}$, GPa (msi) | $E_{2c}$, GPa (msi) | $G_{12}$, GPa (msi) | $\nu_{12}$ | Thickness, mm (in.) |
|---|---|---|---|---|---|---|---|
| IM7/8552 | 161.35 (23.4) | 11.38 (1.65) | 143.4 (20.80) | 12.75 (1.85) | 5.17 (0.75) | 0.32 | 0.152 (0.006) |
| S2/8552 | 47.58 (6.90) | 13.10 (1.9) | 46.88 (6.80) | 17.93 (2.6) | 5.03 (0.73) | 0.27 | 0.152 (0.006) |

Specimens made of two different hybrid lay-ups were studied. The configurations were identical except for the material type used in the plies closest to the midplane. Specimens using graphite/epoxy plies near the mid-plane are designated graphite-midplane specimens (GRMS) and those using glass plies near the midplane are referred to as glass-midplane specimens (GLMS). The exterior taper geometry was the same for both the GRMS and GLMS specimens. Total specimen gage length was 203.2 mm (8-inch) for the GRMS specimens and 165.1 mm (6.5-inch) for the GLMS specimens. The GRMS specimens were tested first with the original 203.2 mm gage length. However, when the GLMS specimens were tested, the gage length was shortened to 165.1 mm to reduce the transverse stroke required to achieve the desired strain levels, and to improve the performance of the test machine. For both gage lengths, the length of the tapered region was 80.7 mm (3.17 in.). The thick region was completely within the bottom grip of the test machine for all test specimens. The nominal specimen dimensions are also shown in fig. 1.

A photograph of the tapered region of a GLMS specimen edge is shown in fig. 2. The figure shows the hybrid materials, as well as the continuous belt-plies and the dropped-ply groups. As the sketch in fig. 2 shows, the terminated plies are dropped in an overlapping pattern so that the plies closest to the midplane are shortest and are terminated first.

The flexbeam specimens were tested in a servo-hydraulic load frame, called the Axial-Tension Bending (ATB) machine. The ATB produces constant axial tension loading under load control, combined with cyclic transverse bending, applied under stroke control. This produces a constant membrane load throughout the loading cycle. Details of the ATB machine can be found in refs. 3 and 9.

Static Tests

Before testing, the specimens were instrumented with back-to-back strain gages along the length of the flexbeam as shown in fig. 1. The specimens were inserted into the lower grip of the test machine so that the thick end was completely within the fixed bottom grip, and the bottom of the tapered region was flush with the top of the lower grip.

Each specimen was tested first under static loading to determine the relationship between applied loads and specimen deflection and surface strains. These relationships were then used to determine the axial load and cyclic transverse displacements for fatigue testing. For static excursions, a constant axial tension load, P, was applied. Then the transverse displacement, $\delta$, was applied, in steps of approximately 2.54 mm (0.1 inch), up to a maximum stroke of 45.7 mm (1.8 inch). At each step, the surface strains along the length were recorded. There was no evidence that the specimen slipped in the grips at any time during the testing.

Fatigue Tests

The axial tension load, P, and transverse displacement, $\delta$, for fatigue testing of each specimen were chosen to simulate the maximum surface strain level in the flexbeam, rather than a maximum flapping angle. Axial tension load was determined by applying a load until the strain in the constant thickness (thin) region at approximately 74 mm from the upper grip reached approximately 2500 $\mu\varepsilon$ , as indicated by gages 3 and 3a in fig. 1. Then, with the axial load held constant, a transverse displacement was applied to correspond to a desired maximum strain level in the tapered region as measured by gages 2 or 2a in fig. 1. This region was chosen for comparison with baseline strain survey data from full-scale flexbeam testing. The maximum strain levels for fatigue testing varied between 4500 $\mu\varepsilon$ and 8000 $\mu\varepsilon$. It should be noted that these loading levels provide accelerated testing and are not representative of component capability or typical flight conditions. Asymmetric loading, with an R-ratio ($\varepsilon_{min}/\varepsilon_{max}$) of approximately R=0.1 was used in this study, rather than fully-reversed loading, to more accurately simulate the loading experienced by the flexbeam in flight. The transverse stroke was applied as a sinusoidal function with a frequency of 3 Hz.

In order to determine the onset of delamination, specimens must be constantly monitored during the fatigue loading. To minimize the effort, and yet to carefully monitor the actual onset of the delamination, a high-speed camera to digitally record the damage progression was assessed in one of the GRMS specimen tests. The system uses a 1K by 1K resolution camera, with a shutter speed of 15 frames/second. The camera was controlled by a computer and was able to digitally record an image at a designated number of loading cycles. Each photograph was taken at the point of maximum transverse deflection of the specimen. Photographs were recorded at every 900 cycles (every 300 seconds). The specimen was also monitored for delamination onset by periodically stopping the cycling and visually checking for damage.

## ANALYSIS

Finite Element Model

In ref. 9, a separate finite element model was developed to represent the GRMS and GLMS flexbeams. The models were identical with the exception of the added length of the thin section of the GRMS model, and the different material properties used for the plies near the midplane. The model was generated using the PATRAN (v8.0) modeling software, and duplicates the nonlinear tapered geometry of the flexbeam and the boundary conditions of the loading apparatus. A schematic of the model is shown in fig. 3,

including a close-up of the finite element representation at a typical ply-ending. The model was 2-D and was symmetric about the midplane. Individual plies were modeled in the outermost dropped ply regions, using square elements and one element per ply. The location of the ply-endings was determined from design drawings. Resin pockets at the tips of each ply-drop region were represented in the model by a right-triangular region as shown in fig. 3. In contrast, the plies near the centerline are coarsely modeled, using three layers of elements on each side of the midplane, and smearing the ply properties in the material definition. The model was analyzed using both the ANSYS and ABAQUS FE codes. A two-dimensional eight-noded plane-strain quadrilateral element with reduced integration was used in both analyses. The ANSYS and ABAQUS codes differ in their implementation of element coordinate systems, orthotropic materials, constraint equations, and solution algorithms. Both codes used a nonlinear solution with stress stiffening, surface-to-surface contact, and large deformation options. The elastic constants given in Table 1 were used with laminated plate theory to determine the three-dimensional orthotropic properties, i.e., x-z plane, required by the analysis codes. Laminated plate theory was also used to calculate smeared properties in the coarsely meshed regions. In order to assign the material properties correctly in the tapered region, the local t-n element coordinate system was used to assign material properties for each element. In ref. 9, a mesh refinement study of this model using ANSYS indicated that a mesh of 1 element per ply was adequate for the analysis using 2-D higher-order elements. For both analysis codes, fixed end conditions were simulated at the thick end of the model. The axial tension load was applied to the free end of the model as a distributed load and the transverse bending was applied as a prescribed displacement.

Strain Energy Release Rate Computation

In order to simulate a crack or delamination in the flexbeam, multi-point constraint (MPC) nodes were incorporated in the model at the ply-ending where delamination onset occurred. Delaminations were then simulated at those interfaces by incrementally releasing the MPCs. The Virtual Crack Closure Technique (VCCT) was used to calculate strain energy release rates at each step of simulated delamination growth. The VCCT uses the forces at the delamination tip, and the relative displacements behind the delamination tip, to calculate the mode I (opening) and mode II (sliding shear) components of strain energy release rate ($G_I$ and $G_{II}$, respectively). The equations for $G_I$ and $G_{II}$; as well as the forces at nodes i and j; and the displacements at nodes l and m, all in the local n-t coordinate system, are shown in fig. 4. These nodal forces and displacements were obtained from the ABAQUS and ANSYS output files. Because these flexbeams experience large deflections, the displacements and forces must be measured in the local coordinate system; i.e., the normal-tangential (n-t) coordinate system for the deformed elements (see fig. 4), rather than the global coordinate system. Details of these calculations are given in refs. 12 and 13. The total strain energy release rate, G, is obtained by summing the individual mode components. Hence, $G = G_I + G_{II}$, since $G_{III}=0$.

## RESULTS AND DISCUSSION

Global Response

In ref. 9, calculated surface strains along the length of the flexbeam under combined tension-bending loading were compared with the measured strains, to determine how well the FE model reproduced the global behavior of the test specimens. The calculated strains from both ABAQUS and ANSYS for the GRMS1 specimen on both the tension and compression sides taken from ref. 9 are shown in fig. 5. The results shown were calculated for an axial load of 42.7 kN (9610 lbs.) and a transverse displacement of 60.7 mm (2.39 inches). The figure shows good agreement between the measured strains and the FE analysis results obtained using the ANSYS and ABAQUS codes. Results for the GLMS model agreed equally well.

Fatigue Tests

Combined tension-bending fatigue testing was performed on three GRMS-type specimens (GRMS1, GRMS2, GRMS3), and four GLMS-type specimens (GLMS1-3 and GLMS6). The prescribed loads and

displacements and the resulting maximum surface strains and R-ratio, for each of the tested flexbeams are listed in Table 2.

Table 2. Flexbeam specimens and test parameters.

| Specimen | Specimen width, mm, (inches) | Transverse displacement, δ, mm (inches) | R-ratio, $\varepsilon_{min}/\varepsilon_{max}$ | $\varepsilon_{max}$, με |
|---|---|---|---|---|
| GRMS1 | 25.4 (1.0) | 48.51 (1.91) | 0.13 | 8000 |
| GRMS2 | 25.4 (1.0) | 20.32 (0.8) | 0.12 | 5000 |
| GRMS3 | 25.4 (1.0) | 22.86 (0.9) | 0.13 | 5658 |
| GLMS1 | 25.4 (1.0) | 33.53 (1.32) | 0.10 | 6830 |
| GLMS2 | 25.4 (1.0) | 27.94 (1.1) | 0.12 | 5600 |
| GLMS3 | 12.7 (0.5) | 43.18 (1.7) | 0.10 | 5756 |
| GLMS6 runout | 12.7 (0.5) | 15.24 (0.6) | 0.11 | 4500 |

The specimens were visually monitored periodically for delamination onset and growth throughout the fatigue loading cycle. Both edges of the specimen were monitored. For all the specimens tested, the initial damage occurred on the "tension" side of the specimen, in the tapered region. The initial damage occurred at approximately 1.5 inches from the lower grip, and near the specimen surface, indicating that, for all specimens, all of the delaminations started at the same ply-drop location, designated ply-ending 311 (see fig.2). Also, damage was visible on both edges of the specimen, (left and right), at the same location, and had the same general appearance, indicating that uniform length delaminations had formed across the width of the specimen.

A representative photo of delamination in specimen GLMS3 after N=61,614 loading cycles is presented in fig. 6. Delaminations can be seen to have started from three distinct ply-drop locations. As the figure indicates, the initial damage occurred at the ply-drop nearest the surface. Delaminations grew toward the thick end of the flexbeam, initially along the interface toward the midplane, and then also along the interface toward the surface. As the loading continued, a second resin crack formed at another ply-drop, and delaminations grew from it toward the thick end, and along both interfaces around the dropped ply. There is also a short delamination along the interface ahead of the resin pocket, toward the thin region. Continued loading resulted in delamination from a third ply-drop. This damage pattern was typical for all the flexbeams tested. In all cases, the delamination growth was very slow and stable. Some tests were allowed to continue until extensive delaminations occurred at multiple interfaces. However, none of the specimens reached an accumulated damage state at which catastrophic failure could occur.

A photomicrograph of the area around ply-ending 311 is shown in fig. 7. The likely delamination interfaces are labeled in fig. 7 as the interface under 311(toward the midplane) labeled interface *bl*, the interface above 311 (toward the surface) labeled interface *b*, or the interface forward from the tip of the resin pocket toward the thin region of the flexbeam, labeled interface *a*. Results for all the tested specimens indicated a preference for growth along interface *bl*, based on experimental observation and delamination length compared to interfaces *a* and *b*.

Digital photographs, as well as visual records of delamination growth, were taken of flexbeam GRMS3 throughout the fatigue test. The photos were examined and the delamination onset and growth results were compared to the visual records. As a result of the visual inspection, damage was clearly detected at ply-ending 311, at N=488,993 cycles. However, the digital images show only a very faint indication that there may be a delamination starting at that point. Damage from the photos was not verifiable until about N=973,528 cycles, when the delamination was already 3-mm long. As the delaminations grew, they became more distinct in the photographs and delaminations developing at other interfaces were easily detected. The camera system proved to be valuable for recording the delamination growth pattern after onset, but was not sufficiently sensitive to detect the onset of delamination at the original site.

Strain Energy Release Rate Analysis

Both the ANSYS and ABAQUS FE analyses were used to calculate the strain energy release rate (SERR) associated with delamination growth in the GRMS and GLMS models. Delaminations were simulated in the models by incrementally releasing multi-point constraints along the delamination interfaces, and calculating the SERR at each increment. The tension crack behind the resin pocket, shown in fig. 7, is simulated to exist in the FE model as the delaminations grow. Details of the SERR calculations can be found in ref. 9.

The SERR calculations for the GRMS model, calculated using ABAQUS, at P=45.52 kN (9560 lbs.) and $\delta$=48.51 mm (1.91 inches), for delamination in each of the three interfaces are shown in fig. 8. These results show that the SERR values are much higher along interface *bl*, indicating that delamination is likely at that interface first. The analysis results also show that delamination along interfaces *bl* and *b* was predominantly mode II, whereas delamination along *a* was entirely mode I. In fig. 9, SERR results along interface *bl*, obtained from the ANSYS and ABAQUS analyses, are compared for the GRMS model. Results from the two methods are almost identical. As the figure shows, along the *bl* interface, the SERR increases very rapidly to a peak value as the delamination grows under the dropped ply. As the delamination continues to grow, it encounters another resin pocket, and the SERR drops sharply as the delamination grows under that resin pocket, then increases to a second peak value as the delamination reaches the next dropped ply. The corresponding results for the GLMS model along interface *bl* are presented in fig. 10. Again, the ABAQUS and ANSYS results are very similar; at the initial peak the ABAQUS results are approximately 3.4 % higher. In ref. 9, SERR results from ABAQUS and ANSYS analyses for the GRMS model were shown to differ by 5 to 11% throughout the delamination growth. In this report, an element with reduced integration was used with the ABAQUS analysis which resulted in improved correlation between the two analyses.

The ABAQUS and ANSYS calculated mode II percentages of the SERR along interface *bl*, for both the GRMS and GLMS specimens, are presented in fig. 11. For both models, the initial delamination growth is entirely mode II. As the delamination grows to the second resin pocket, the percentage of mode II drops to about 95%.

Delamination Onset Prediction

In refs. 3, 9, and 14, peak values of calculated strain energy release rates, from curves like those shown in figs. 9 and 10, were used with measured G vs. N data from material characterization tests to calculate a curve that relates delamination onset and the number of loading cycles. A similar approach was used here to generate a curve that relates the maximum surface strain to the number of cycles to delamination onset. The G vs. N results for the IM7/8552 graphite/epoxy material from mode II (4ENF) tests, where a curve of the form $G_{max}(N)=1307.8N^{-0.16463}$ was fit through the data is shown in fig. 12. Because the initial delamination growth was entirely mode II, this curve was considered acceptable for predicting delamination onset along the *bl* interface. Then it was assumed that delamination would initiate in the test specimens when the peak G-value from the FE analysis equaled the cyclic $G_{IImax}$ at which delamination started in the 4ENF specimens. That is,

$$\left[\frac{G_{FE}}{V_{FE}^2}\right] = \frac{G_{IImax}}{V^2}$$

where $G_{FE}$ is the peak G for delamination along *bl*, and $G_{IImax}$ is the equation fit to the 4ENF data. The term $V_{FE}$ corresponds to the applied transverse displacement in the model. The equation can be re-written to solve for V, the applied transverse load. By relating the applied transverse load to the maximum surface strain, a calculated curve can be generated relating the maximum surface strain to the number of cycles for delamination onset. More details of this procedure are found in ref. 3. The calculated curve for

the GRMS flexbeam is shown in fig. 13, along with test results for the 3 GRMS-type specimens. As noted on the figure, the GRMS1 specimen already showed significant delamination growth when it was first checked at 2900 cycles, and therefore the data point shown is not truly the onset location, but after some damage had accumulated. Results for the GLMS-type specimens are shown in fig. 14. The test results agree reasonably well with the calculated curves. The GLMS6 specimen is shown as a runout, since testing was terminated at 2 million cycles, with no delamination detected.

In ref. 14, the cumulative life to failure ($N_T$) is defined as the sum of the number of cycles to the onset of matrix cracking ($N_M$), the number of cycles to delamination onset from the matrix crack ($N_D$), and the number of cycles to grow the delamination to a limiting size ($N_G$). However, this study was not concerned with growth to a finite limiting delamination length, $N_G$. The life prediction curves shown in figs. 13 and 14 are calculated assuming that there is an existing resin pocket crack. That is, the calculated life is from the development of the resin crack to delamination onset ($N_D$), but does not include the number of cycles to cause the resin crack itself to form ($N_M$). However, it should be noted that, for the coupon flexbeams tested for this study, matrix cracking without any associated delamination growth was never observed. Hence, it is possible that, for these flexbeams, matrix cracking and delamination onset occur simultaneously.

## CONCLUDING REMARKS

Nonlinear -tapered flexbeam laminates were cut from a full-size composite helicopter rotor hub flexbeam and were tested under combined constant axial tension and cyclic bending loads. Two different graphite/glass hybrid configurations were studied. The terminated plies were dropped in an overlapping stepwise pattern. All of the specimens failed by delaminations first starting as a matrix crack at the tip of the ply drop group in the tapered region, and growing at the interfaces around the dropped ply toward the thick region of the flexbeam. As the cyclic loading was continued, delaminations continued to grow and new delaminations formed at multiple interfaces. A 2-D finite element model was developed which closely approximated the flexbeam geometry, boundary conditions, and loading. The model was analyzed using two geometrically nonlinear FE codes, ANSYS and ABAQUS. Delaminations of various lengths were simulated in the analytical model by releasing multipoint constraints (MPCs). Strain energy release rates (G) were calculated using the virtual crack closure technique (VCCT) using both ANSYS and ABAQUS. The calculated peak G values were used with material characterization data to calculate fatigue life curves, for comparison with test data. An automated digital camera system was evaluated for its ability to detect delamination onset in the flexbeams. The following observations were made based on the results:

1. Delaminations originated at the tip of the 311 ply-ending group and tended to grow toward the thick end of the flexbeam. Delamination was allowed to accumulate at multiple interfaces without catastrophic failure of the flexbeam.
2. A digital camera system was not sufficiently sensitive to detect the onset of delamination from the resin crack.
3. Calculated G-values from the ANSYS and ABAQUS FE codes were nearly identical for delamination growth along the primary delamination interface, for both hybrid specimen types.
4. Both FE analysis results suggest that the initial delamination growth from the resin crack toward the thick region of the flexbeam is dominated by mode II.
5. A curve relating maximum surface strain to the number of loading cycles at delamination onset was calculated for each hybrid specimen type. Test results compared reasonably well with the calculated results. The calculations predict the fatigue life from the opening of the resin crack until delamination onset, but do not include the cycles necessary to open the resin crack initially. Observations from the testing indicated that delamination onset occurred shortly after, or simultaneously with, the development of the resin crack.

## REFERENCES


(1) O'Brien, T. K., "Towards a Damage Tolerance Philosophy for Composite Materials and Structures," *Composite Materials: Testing and Design, Vol. 9, ASTM STP 1059*, S. P. Garbo, Ed., American Society for Testing and Materials, Philadelphia, 1990, pp. 7-33.

(2) Martin, R. H., "Incorporating Interlaminar Fracture Mechanics into Design," International Conference on Designing Cost- Effective Composites, ImechE Conference Transactions, London, September 15-16, 1998, pp. 83-92.

(3) Murri, G. B., O'Brien, T. K., and Rousseau, C. Q., "Fatigue Life Methodology for Tapered Composite Flexbeam Laminates," *Journal of the American Helicopter Society*, Vol. 43, No. 2, April 1998, pp. 146-155.

(4) Fish, J. C. and Lee, S. W., "Tensile Strength of Tapered Composite Structures," AIAA Paper No. 88-2252, *Proceedings of the 30th AIAA/ASME/ASCE/AHS Structures, Structural Dynamics and Materials (SDM) Conference*, Williamsburg, VA, April 1988, pp. 324-333.

(5) Hoa, S. V., Daoust, J., and Du, B. L., "Interlaminar Stresses in Tapered Laminates," *Polymer Composites*, Vol. 9, No. 5, October 1988, pp. 337-344.

(6) Llanos, A. S., Lee, S. W., and Vizzini, A. J., "Delamination Prevention in Tapered Composite Structures under Uniaxial Tensile Loads," AIAA Paper No. 90-1063, *Proceedings of the 31st AIAA/ASME/ASCE/AHS Structures, Structural Dynamics and Materials (SDM) Conference*, Long Beach, CA, April 1990, pp. 1242-1252.

(7) Murri, G. B., Salpekar, S. A., and O'Brien, T. K., "Fatigue Delamination Onset Prediction in Unidirectional Tapered Laminates," *Composite Materials: Fatigue and Fracture (Third Volume), ASTM STP 1110*, T. K. O'Brien, Ed., American Society for Testing and Materials, Philadelphia, 1991, pp. 312-339.

(8) Wisnom, M. R., "Delamination in Tapered Unidirectional Glass Fibre-Epoxy Under Static Tension Loading," AIAA Paper No. 91-1142, *Proceedings of the 32nd AIAA/ASME/ASCE/AHS Structures, Structural Dynamics and Materials (SDM) Conference (Part 2)*, Baltimore, MD, April 1991, pp. 1162-1172.

(9) Murri, G.B., Schaff, J.R., and Dobyns, A. L., "Fatigue and Damage Tolerance of a Hybrid Composite Tapered Flexbeam," Proceedings of the American Helicopter Society, Forum 54, Washington, D.C., May 2001.

(10) ANSYS/Mechanical, Version 6.1, ANSYS, Inc., 1999.

(11) ABAQUS/Standard, Version 5.8-14, Hibbitt, Karlsson, and Sorensen, Inc., 1999.

(12) Rybicki, E. F. and Kanninen, M. F., "A Finite Element Calculation of Stress Intensity Factors by a Modified Crack Closure Integral," *Engineering Fracture Mechanics*, Vol. 9, 1977, pp. 931-938.

(13) Raju, I. S., "Simple Formulas for Strain Energy Release Rates with Higher Order and Singular Finite Elements," NASA Contractor Report 178186, December 1986.

(14) Krueger, R., Paris, I. L., O'Brien, T. K., and Minguet, P. J., "Fatigue Life Methodology for Bonded Composite Skin/Stringer Configurations," JCTR, Vol. 24, 2002, pp. 56-79.

(15) Hansen, P., and Martin, R., "DCB, 4ENF, and MMB Delamination Characterisation of S2/8552 and IM7/8552," Materials Engineering Research Laboratory Ltd. (MERL), Hertford, U.K., N68171-98-M-5177, 1999.

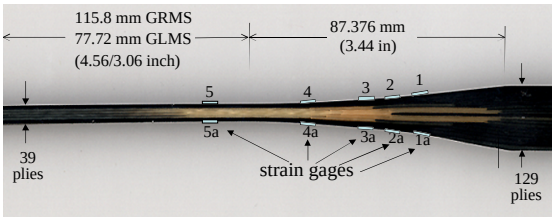


Figure 1. Tapered hybrid flexbeam specimen with net dimensions and strain gage locations.

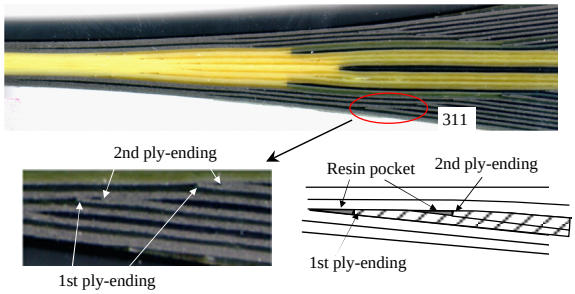


Figure 2. Edge of tapered hybrid composite specimen showing dropped plies.

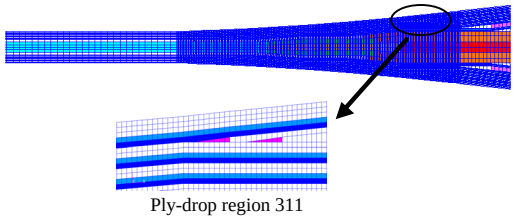


Figure 3. Finite element model of flexbeam and ply–drop region.

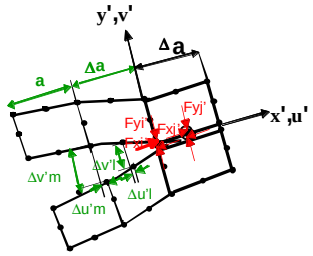


$$G_I = \frac{1}{2\Delta a}\left(F'_{yi}\,\Delta v'_m + F'_{yj}\,\Delta v'_l\right) \qquad G_T = G_I + G_{II}$$

$$G_{II} = \frac{1}{2\Delta a}\left(F'_{xi}\,\Delta u'_m + F'_{xj}\,\Delta u'_l\right)$$

Figure 4. Virtual Crack Closure Technique in local coordinate system [14].

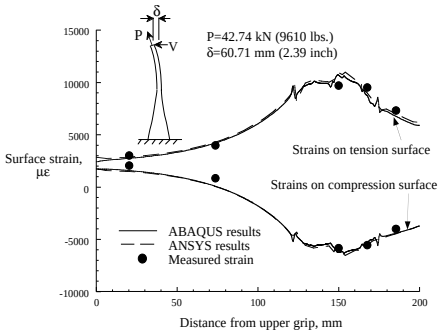


Figure 5. Comparison of measured and calculated surface strains in GRMS flexbeam.

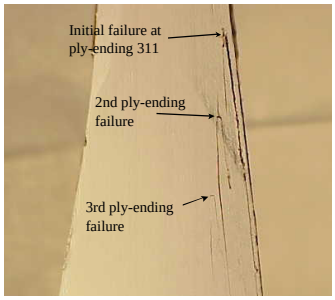


Figure 6. Delamination damage in GLMS3 specimen at N==61,614 cycles.

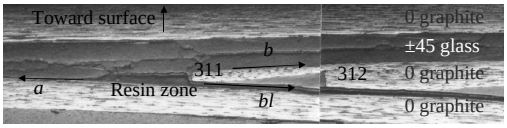


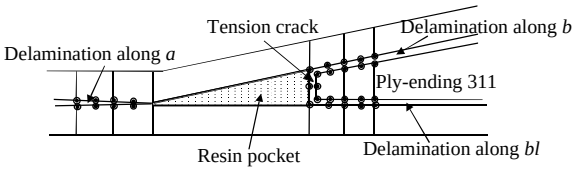


Figure 7. Delamination at ply-ending 311 and three possible paths for delamination growth.

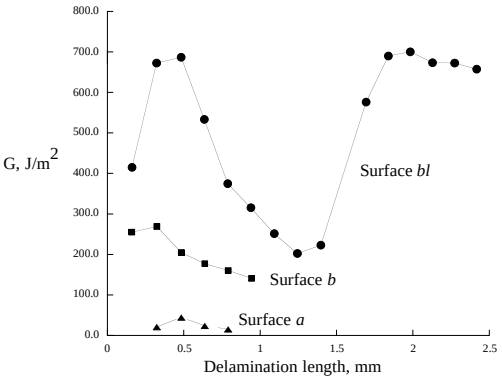


Figure 8. Strain energy release rates for delamination at 3 interfaces in GRMS flexbeam.

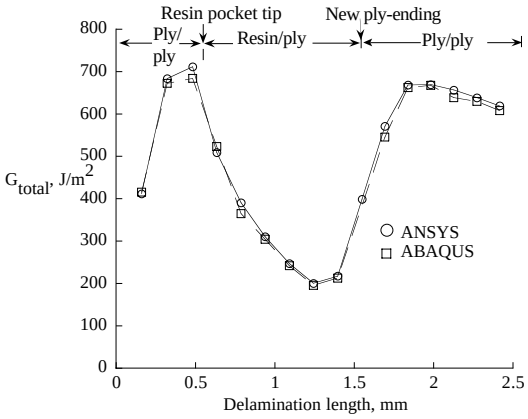


Figure 9. Calculated strain energy release rate results for delamination along interface *bl* in GRMS flexbeam.

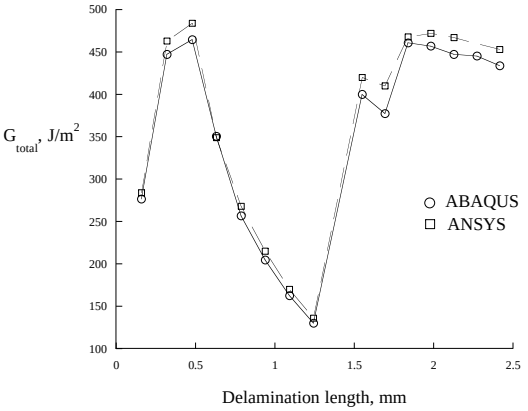


Figure 10. Calculated strain energy release rate results for delamination along interface *bl* in GLMS flexbeam.

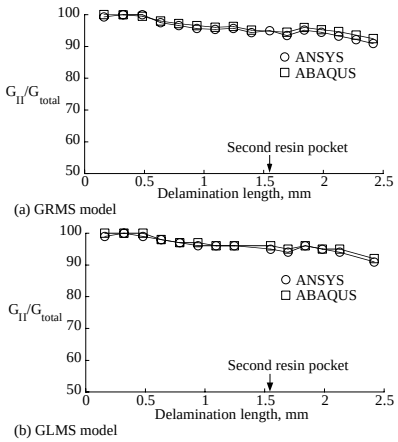


Figure 11. Calculated mode II percentage for delamination along interface *bl* in GRMS and GLMS flexbeams.

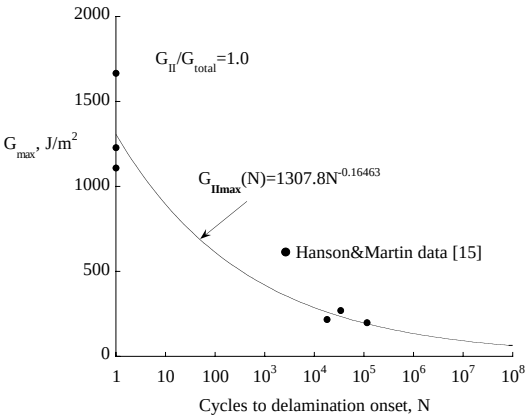


Figure 12. Delamination onset data and fitted curve for cyclic mode II 4ENF tests of graphite/epoxy material.

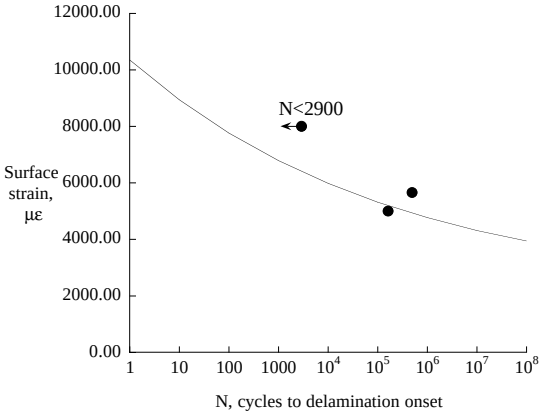


Figure 13. Calculated and measured delamination onset for GRMS flexbeams.

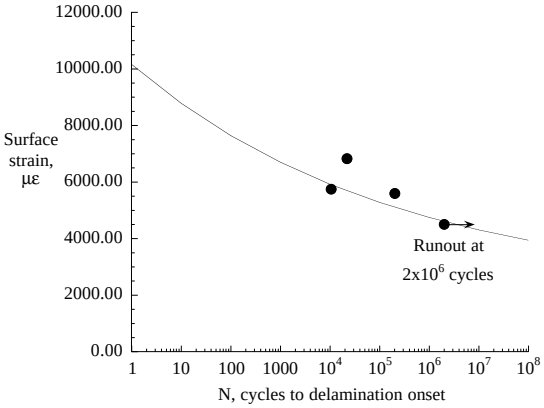


Figure 14. Calculated and measured delamination onset for GLMS flexbeams.